Electronic Properties of the 2,6-Diiododithieno[3,2-*b*:2′,3′-*d*]thiophene Molecule and Crystal: A Joint Experimental and Theoretical Study

Roel S. Sánchez-Carrera,[†,‡] Susan A. Odom,[†,§] Tiffany L. Kinnibrugh,[‖] Tissa Sajoto,[†] Eung-Gun Kim,[†] Tatiana V. Timofeeva,[‖] Stephen Barlow,[†] Veaceslav Coropceanu,[†] Seth R. Marder,*[,†] and Jean-Luc Brédas*[,†]

School of Chemistry and Biochemistry and Center for Organic Photonics and Electronics, Georgia Institute of Technology, Atlanta, Georgia 30332-0400, and Department of Natural Sciences, New Mexico Highlands University, Las Vegas, New Mexico 87701

The electronic properties of the 2,6-diiododithieno[3,2-*b*:2′,3′-*d*] thiophene molecule and crystal are investigated by means of UV−vis spectroscopy, cyclic voltammetry, X-ray crystallography, and density functional theory. The experimental and calculated properties of the compound are compared to those exhibited by the parent molecule, dithieno[3,2-*b*:2′,3′-*d*]thiophene. Quantum-chemical studies of the 2,6-diiododithieno[3,2-*b*:2′,3′-*d*]-thiophene crystal suggest uniaxial hole-transport character with an effective mass of about $2m_0$, comparable to that in the pentacene single crystal.

I. Introduction

Organic field-effect transistors (OFETs) are attracting a great deal of attention for use in large-area and/or flexible applications.[1−4] Some of the most widely investigated molecular materials in organic electronics are those belonging to the oligoacene[1,2] and oligothiophene[3−5] families. Among them, pentacene[6] and α-sexithienyl[7,8] have been of special interest due to their relatively high charge-carrier mobilities. Much effort has been devoted to the design of environmentally stable fused aromatic derivatives with high charge-carrier mobilities,[1,9−12] and dithieno-[3,2-*b*:2′,3′-*d*]thiophene (DTT) has been widely used as a building block for molecular and polymeric compounds, in particular for hole-transport materials.[13−18]

Recently, large hole mobility values, up to 12 cm²/(V·s) at room temperature, have been confirmed in crystals of 1,4-diiodobenzene (DIB).[19] Our earlier theoretical work suggests that the origin of such a high mobility is primarily associated with the presence of the heavy iodine atoms.[20] These results inspired us to investigate the properties of an iodinated version of DTT: 2,6-diiododithieno[3,2-*b*:2′,3′-*d*]thiophene (DTT-2I). Here, we report the main electronic and optical characteristics of the compound in solution (from UV−visible absorption spectroscopy and cyclic voltammetry), the crystal structure, and quantum-chemical calculations of the electronic properties of the molecular crystal.

II. Results and Discussion

a. Molecular Properties. DTT-2I was synthesized from the iodination of DTT (obtained using a method published by Holmes et al.[21]) with *N*-iodosuccinimide in chloroform/acetic acid solution (see the Experimental Section for complete details).
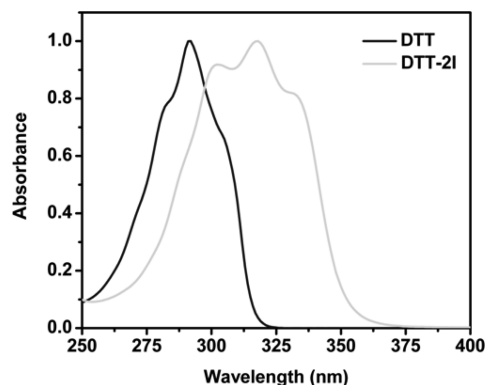
Figure 1. UV−vis absorption spectra of DTT and DTT-2I in dichloromethane.

X-ray quality crystals were grown from a toluene solution. The melting point of DTT-2I (ca. 160 °C) is higher than that of DIB (131 °C) and DTT (ca. 65 °C).

Figure 1 shows the absorption spectra of DTT and DTT-2I in dichloromethane. Both spectra are structured, which indicates a strong coupling of the excitation with high-frequency vibrational modes. Iodine substitution results in a red shift of the absorption maxima by roughly 0.35 eV, which is consistent with iodine atoms acting as π-electron donors (see below).[22]

Time-dependent density functional theory (TDDFT) calculations indicate that the first optical band is dominated by the $S_0 \rightarrow S_1$ transition, though a weak contribution from excitation into the S_2 state located about 0.2 eV above S_1 is also predicted. In DTT-2I, the first optical band is dominated by the $S_0 \rightarrow S_3$ transition. The TDDFT energies of 4.32 and 3.89 eV calculated for the S_1 state in DTT and the S_3 state in DTT-2I, respectively, are in good agreement with the energies of the corresponding absorption maxima, 4.25 and 3.90 eV.

In the context of a one-electron approximation, the S_1 state in DTT and S_3 state in DTT-2I can both be described predominantly as HOMO-to-LUMO excitations. The DFT-derived frontier molecular orbitals are shown in Figure 2. Iodine substitution results in a HOMO−LUMO energy gap in DTT-

* To whom correspondence should be addressed. E-mail: seth.marder@gatech.edu (S.R.M.); jean-luc.bredas@chemistry.gatech.edu (J.-L.B.).
† Georgia Institute of Technology.
‡ Present address: Department of Chemistry and Chemical Biology, Harvard University, Cambridge, Massachusetts 02138.
§ Present address: Department of Chemistry, University of Illinois at Urbana−Champaign, Urbana, Illinois 61801.
‖ New Mexico Highlands University.
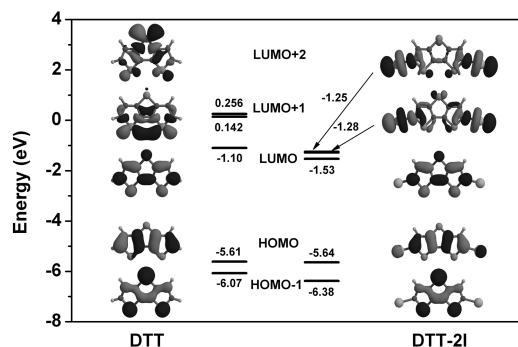
Figure 2. Illustration of the frontier molecular orbitals of DTT and DTT-2I.
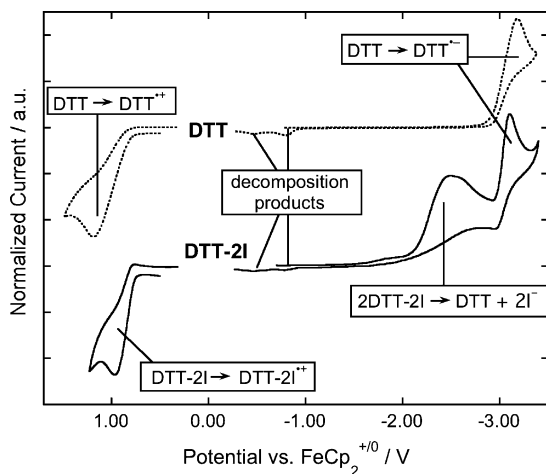
Figure 3. Oxidative (left) and reductive (right) cyclic voltammograms of DTT (upper) and DTT-2I (lower) recorded in DMF/0.1 M $^nBu_4NPF_6$ at 100 mV s^{-1} with proposed assignments of features (see text).

Figure 4. DFT geometries (bond lengths in Å) for the neutral, radical-cation, and radical-anion states of DTT-2I.

2I ca. 0.4 eV smaller than in DTT, which is essentially due to a stabilization of the LUMO level. Iodine atoms play a dual role, being π-donors from a mesomeric standpoint and σ-acceptors from an inductive standpoint. The inductive effect dominates in the case of the LUMO, which stabilizes, while the mesomeric and inductive effects compensate one another in the case of the HOMO.

The electrochemical properties of DTT and DTT-2I were investigated in DMF/0.1 M $^nBu_4NPF_6$. The oxidative behavior is qualitatively rather similar: DTT and DTT-2I both undergo EC-type oxidations (i.e., reversible electron-transfer processes followed by a chemical reaction of the oxidized species on a comparable time scale) at half-wave potentials, $E_{1/2}$, of approximately +0.98 and +0.89 V, respectively, vs ferrocenium/ferrocene (Figure 3). The reductive behavior of the two species is very different. DTT undergoes an EC-type reduction at $E_{1/2}$ = −3.04 V vs ferrocenium/ferrocene; following scanning of this reduction, additional features appear in the oxidative scan at peak potentials of −0.80 and −0.48 V and are presumably due to decomposition products resulting from the reaction of the dithienothiophene radical anion. A reductive scan of DTT-2I, on the other hand, shows an irreversible feature at an apparent peak potential, E_{red}, of −2.40 V (at 100 mV s^{-1}, shifted to a more cathodic potential at faster scan rates), followed by an EC-type feature at a potential essentially identical to that seen for DTT itself, with a 2:1 ratio in the integrated areas for these two reduction waves. Moreover, after scanning the irreversible reduction at −2.40 V, oxidative scans show the presence of DTT as well as DTT-2I in the solution. Accordingly, we propose that the following processes occur during the reduction of DTT-
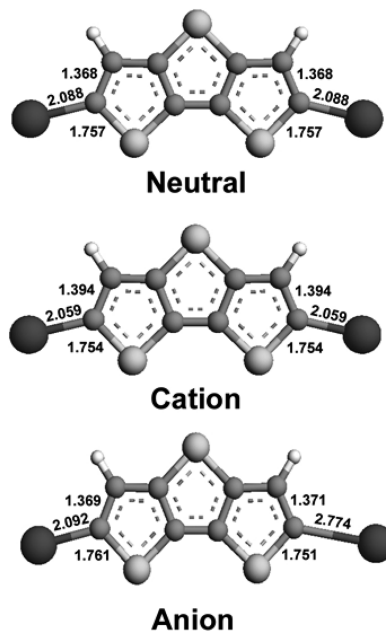
2I. Initial reduction is coupled to C−I bond cleavage to give an iodide anion and a radical which abstracts H• (presumably from the solvent) to give 2-iododithienothiophene, which itself undergoes an analogous reductive deiodination process to give DTT, the EC reduction of which is then observed at −3.04 V (and the oxidation of which is observed in the oxidative scans). Similar electrochemical deiodination processes have been observed for other iodinated derivatives of aromatic ring systems.[23−25] Indeed, a series of substituted iodobenzenes is found to exhibit a rather similar E_{red} value of ca. −2.4 V, similar to that for DTT-2I, in DMF.[25,26]

Quantum-chemical calculations provide a further understanding and are broadly consistent with the experimental observations. An interesting feature is that, while many of the orbitals of DTT-2I closely resemble the corresponding orbitals in DTT, the LUMO+1 and LUMO+2 in DTT-2I lie energetically very close to the LUMO, and are essentially localized C−I σ* orbitals. When maintaining the symmetrical geometry of the neutral species, the electronic structure of the radical-anion ground state (see Figure S1 in the Supporting Information) has an extra electron present on the LUMO (here, we use the orbital notation of the neutral state); the first excited state of the anion, which arises from a LUMO to either LUMO+1 or LUMO+2 excitation, is doubly degenerate and is located only 0.3 eV above the ground state. However, the DFT calculations further show that, in contrast to the oxidized (radical-cation) state where the symmetric geometry of the neutral state is preserved, reduction of DTT-2I results in an extreme elongation (by about 0.7 Å, see Figure 4) of one of the C−I bonds and induces the localization of the unpaired electron in the related localized C−I σ* orbital. This broken-symmetry state apparently has only a small barrier to C−I bond cleavage.

The electrochemical data suggest that the condensed-phase ionization potentials (IPs) of DTT and DTT-2I are likely to be similar; these values are estimated as 5.8 and 5.7 eV, respectively, using the reference value of 4.8 eV for ferrocene.[27,28] DFT estimates of the vertical gas-phase IPs of DTT and DTT-2I are 7.4 and 7.1 eV, respectively. The value for DTT is close to the previously reported experimental UPS values of 7.55 eV (adiabatic) and 7.78 eV (vertical).[29] It is well-known that solid-
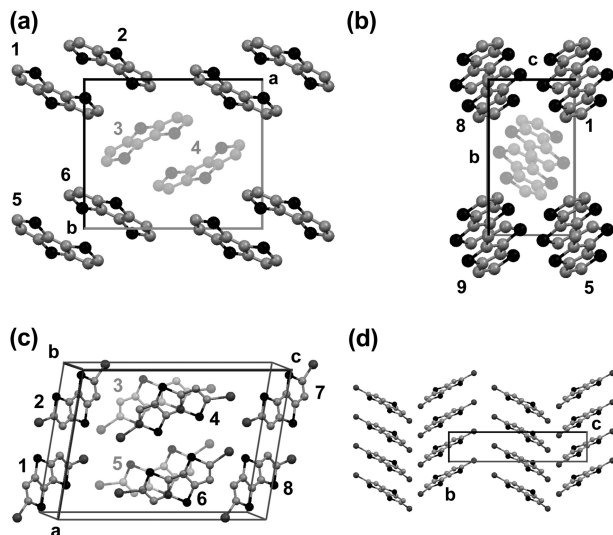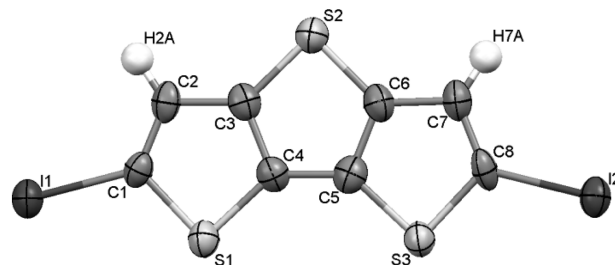
Figure 5. Top: Crystal structure of DTT[31] viewed along the *ab* (a) and *bc* (b) planes (*a* = 12.746, *b* = 10.614, *c* = 6.005 Å; *β* = 97.53°). Bottom: Crystal structure of DTT-2I viewed along the *ac* (c) and *bc* (d) planes (*a* = 13.200, *b* = 4.140, *c* = 19.760 Å; *β* = 96.354°). The labeling of the DTT and DTT-2I molecules used in the calculations of the transfer integrals is also shown.

Figure 6. Molecular structure of DTT-2I from its single-crystal X-ray structure (50% thermal ellipsoids). Selected bond lengths (Å): C1−I1 2.099(10), C8−I2 2.091(10), C1−S1 1.743(11), C8−S3 1.740(10), C1−C2 1.328(16), C3−C4 1.353(17).

Figure 7. Calculated electronic band structure of the DTT crystal. The valence band edge is located at the Γ-point. The right panel illustrates the corresponding density of states. The high-symmetry points in units of (*a**, *b**, *c**) are Γ = (0,0,0), *A* = (0.5,0.5,0), *B* = (0.5,0,0), *C* = (0,0.5,0.5), *Y* = (0,0.5,0), and *Z* = (0,0,0.5).

Figure 8. Calculated electronic band structure of the DTT-2I crystal. The valence band edge is located at *A* = (0.5,0.5,0). The right panel illustrates the corresponding density of states. The high-symmetry points in units of (*a**, *b**, *c**) are Γ = (0,0,0), *A* = (0.5,0.5,0), *B* = (0.5,0,0), *C* = (0,0.5,0.5), *Y* = (0,0.5,0), and *Z* = (0,0,0.5).

state IPs are smaller than gas phase values due to the contribution of polarization energy;[30] the solid-state polarization energy of DTT, from a comparison of solid-state and gas-phase photoelectron spectroscopy measurements, is about 1.6 eV.[29] Assuming a similar polarization energy for DTT-2I and applying these polarization energies to the DFT gas-phase values, we reach values for the solid-state IPs of these compounds similar to those estimated from the electrochemical data. These results point to the fact that fairly large hole-injection barriers from electrodes such as gold should be anticipated for DTT and DTT-2I.
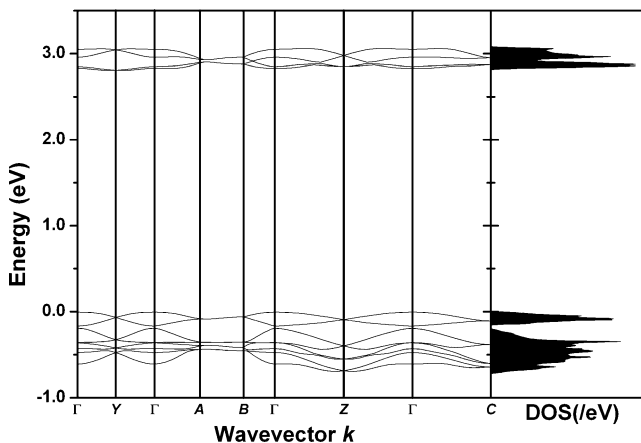
The solid-state EAs can be roughly estimated as −1.8 and −2.2 eV for DTT and DTT-2I, respectively, from the IPs in combination with the onsets of the absorption spectra shown in Figure 1 (a procedure which provides an upper bound for the EAs). The estimated values suggest that injection barriers in a device using gold electrodes would be larger than those observed in the case of hole injection. Furthermore, any C−I cleavage in the solid state, analogous to that observed for DTT-2I in solution, would likely hinder the use of DTT-2I as an electron-transport material.

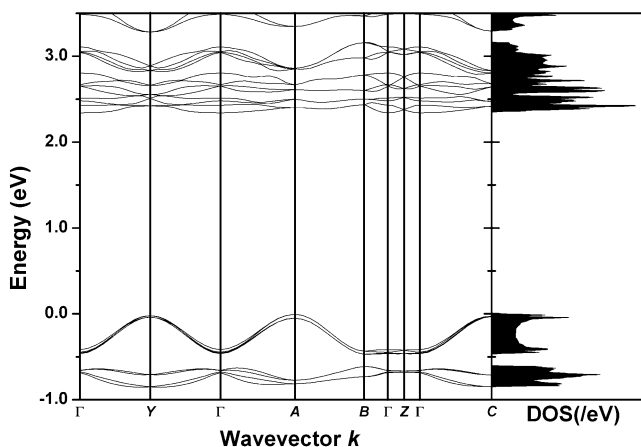**b. Crystal Structure and Electronic Band Structure.** Figure 5 illustrates the packing in DTT, from the previously reported crystal structure,[31] and in DTT-2I, from the crystal structure determined in this work. Figure 6 shows the molecular structure of DTT-2I and lists a number of bond lengths for comparison with those from the DFT-minimized structure (Figure 4). Both compounds crystallize in the $P2_1/n$ space group with one molecule comprising the asymmetric unit, so that both unit cells consist of four translationally inequivalent molecules. As seen from Figure 5a, DTT exhibits a dimerized, pyrene-like[30] structure in the *ab* plane. However, in contrast to the pyrene crystal, the molecular pairs forming the herringbone pattern in DTT are located in separate *ab* planes. The main difference between the crystal structures of DTT-2I and DTT is the presence in DTT-2I of a dense π-stacking pattern along the *b*-axis; a similar π-stacking feature is also observed along the *b*-axis in the α,α′-bis(dithieno[3,2-*b*:2′,3′-*d*]thiophene) (bis-DTT) crystal.[16]

The electronic band structures of DTT and DTT-2I are shown in Figures 7 and 8. The zero of energy corresponds to the valence band maximum. Given that the radical anion of DTT-2I is expected to be unstable in the solid state, we focus here on the hole-transport properties.

The width of the top valence band in the DTT crystal, as follows from the inspection of the calculated density of states, is about 0.17 eV. This band results from the interactions among the HOMO manifold. However, as seen from Figure 7, instead of the four sub-bands expected from the presence of four

TABLE 1: DFT Estimates of the Transfer Integral for Molecular Pairs Extracted from the DTT Crystal (See Figure 5a and b for Labeling)

	hole (meV)	electron (meV)
$t_{1,2}$; $t_{3,4}$; $t_{5,6}$	−138	18
$t_{1,3}$	19	39
$t_{2,3}$	54	21
$t_{1,8}$; $t_{5,9}$	6	1

TABLE 2: DFT Estimates of the Transfer Integral for Molecular Pairs Extracted from the DTT-2I Crystal (See Figure 5c for Labeling)

	hole (meV)	electron (meV)
$t_{1,2}$	−7	1
$t_{1,3}$; $t_{6,7}$	5	−4
$t_{1,4}$; $t_{5,7}$	−1	10
$t_{2,4}$; $t_{6,8}$	−1	5
$t_{3,4}$	−122	1
$t_{4,7}$	−7	−1

nonequivalent molecules in the unit cell, the top valence band consists of only two sub-bands; the other two sub-bands are actually incorporated within the next valence band, which appears to consist of six sub-bands. This finding can be rationalized on the basis of the evaluation of the transfer integrals (see Table 1). According to these calculations, there are very large electronic couplings among translationally inequivalent molecules forming the molecular pairs in the *ab* plane (for instance, pairs formed by molecules 1 and 2 or molecules 3 and 4). On the other hand, the electronic interactions between molecules in these pairs and other molecules are much weaker; in fact, the largest coupling among translationally equivalent molecules is only about 6 meV. These results suggest that the significant coupling found within the molecular dimers mostly contributes to band splitting rather than to band dispersion: the four subbands split into two groups; two subbands form the top valence band, while the other two subbands mix with the HOMO-1 manifold and form the next valence band (we note that the HOMO-1 level in the DTT molecule is separated from the HOMO level by 0.4 eV; this value is comparable to the intermolecular resonance interaction energy within a dimer, for instance, $4t_{12} = 0.55$ eV).

In the DTT-2I crystal, the top valence band is very different from that in DTT, as it consists of four nearly degenerate subbands and has a width of 0.47 eV. The calculated transfer integrals for molecular dimers of the DTT-2I crystal are summarized in Table 2. In contrast to DTT, strong electronic couplings occur between molecules in the π-stacks along the *b*-axis and hardly any coupling exists among translationally inequivalent molecules (which explains the 4-fold degeneracy of the valence band). We note that the bandwidth of 0.47 eV obtained along the *b* (π-stacking) direction from band structure calculations is in excellent agreement with the related value of $4t_{3,4} = 0.49$ eV that would be derived in the framework of a one-dimensional tight-binding model. As expected from the similarity in crystal structures, the electronic interactions in bis-DTT[32] exhibit the same pattern as in DTT-2I; however, the DFT estimate for the electronic coupling along the π-stacking direction is about 50% larger in bis-DTT (180 meV) than in the DTT-2I crystal.

In the case of wide bands, where the thermally populated levels remain close to the band edges, the description of charge transport can be simplified by using the electron effective mass approximation. The tensor for the inverse effective mass (m_{ij}) is given by

$$m_{ij}^{-1} = \frac{1}{\hbar^2} \frac{\partial^2 \varepsilon}{\partial k_i \partial k_j} \qquad (1)$$

Here, subscripts i and j denote the Cartesian coordinates in reciprocal space, ε the band energy, $\hbar$ the Planck constant, and k the momentum. Using eq 1, we calculated the effective masses for hole charge carriers in the DTT and DTT-2I crystals; their values are shown in Table 3.

The smallest mass for holes in DTT ($3.7m_0$) is found along the diagonal direction in the *ac* plane. Such an effective mass is significantly larger than that calculated for other organic molecular crystals used in charge-transport applications, such as pentacene.[33] In the DTT-2I crystal, the lightest holes ($2.0m_0$) are found as expected along the *b*-axis. It is interesting to point out that, in the framework of a tight-binding model, the effective mass for holes along the π-stacking direction is estimated to be only 30% smaller in bis-DTT than in DTT-2I ($1.4m_0$ vs $1.8m_0$); experimental data indicate that the room-temperature hole mobility in bis-DTT thin films is in the range 0.02−0.05 cm²/(V·s).[16]

The calculations also show that, along the *c*-axis, where the intermolecular distances between iodine atoms are shortest (~3.9 Å), the effective mass is very large ($76m_0$). This finding is in marked contrast with what was calculated in the 1,4-diiodobenzene crystal;[20] there, the lightest effective masses are found along the axis with the shortest intermolecular distances between its halogen atoms.

c. Electron−Vibration Coupling. In organic molecular crystals, there are two major sources of electron−phonon (electron−vibration) interactions that affect the microscopic charge-transport properties of these materials:[30,34−36] the so-called *local* coupling, due to the modulation of the site energies (roughly speaking, the HOMO and LUMO energies) by intra- and intermolecular vibrations, and the *nonlocal* coupling, due to the modulation of the transfer integrals by intermolecular vibrations. It is now widely accepted that both local and nonlocal electron−vibration couplings must be taken into account in order to obtain a comprehensive description of charge transport in organic molecular crystals.[35] Some recent reports have demonstrated the effect of nonlocal coupling on the vibration-assisted contribution to charge transport in the naphthalene crystal.[37−40]

The overall strength of the local vibrational coupling is expressed by the reorganization energy, λ, upon ionization (appearance of a charge carrier on a molecule), which arises from the changes in the geometry of the individual molecules and from the polarization of the surrounding molecules. Since recent theoretical calculations[41] have shown that the polarization contributions are expected to be very small, we focus mainly on the description of the intramolecular geometry relaxation contributions to the local coupling.

The intramolecular reorganization energy calculated for DTT-2I (271 meV) is nearly 20% smaller than that in DTT (353

TABLE 3: Hole Effective Masses M (in Units of the Electron Mass at Rest, m_0) Calculated at the Band Edges of the DTT and DTT-2I Crystals

DTT	m/m_0	parallel to
holes at Γ	3.73	$a + 0.813c$
	7.16	b
	12.10	$c − 0.152a$

DTT-2I	m/m_0	parallel to
holes at A	8.47	$a + 0.095c$
	1.99	b
	75.52	$c + 0.035a$

Electronic Properties of DTT-2I

J. Phys. Chem. B, Vol. 114, No. 2, 2010 **753**
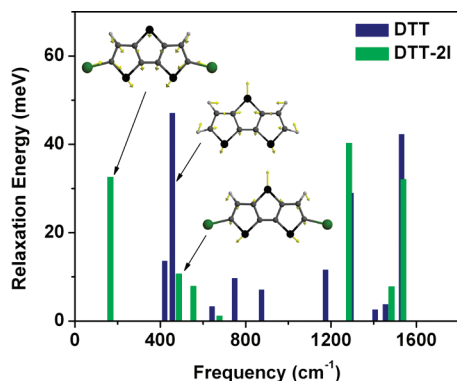
Figure 9. Contributions of the vibrational modes to the relaxation energy upon ionization of DTT and DTT-2I.

SCHEME 1: Synthesis of DTT-2I
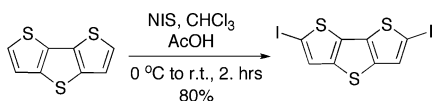
meV), and is approximately 3 times larger than that estimated for pentacene (97 meV).[42] The intramolecular reorganization energy consists of two terms related to the geometry relaxation energies upon going from the neutral-state geometry to the charged-state geometry and vice versa.[42] The DFT calculations reveal that these two contributions to the reorganization energy are nearly identical in both DTT and DTT-2I (see Tables S1 and S2 in the Supporting Information for more details), as found for many other systems.[42,43] In Figure 9, we illustrate the contribution of each vibrational mode to the relaxation energy related to the formation of the radical-cation state. The decrease of λ in DTT-2I versus DTT comes from a drop in hole−vibration coupling with several modes in the range 400−1200 cm^{-1}. The decrease in hole−vibration interaction in DTT-2I can be understood in terms of the orbital vibronic coupling constants.[44,45] According to this model, the hole−vibration coupling is large when the molecular deformation along a normal coordinate considerably distorts the electron density of the related molecular orbital (in this case of the HOMO), leading to a large variation in the orbital energy. In DTT-2I, a portion of the electron density of the HOMO is located on the iodine atoms that, due to their large masses, remain nearly motionless during molecular vibrations. As a result, the hole−vibration coupling constants of the modes involving the iodine atoms are reduced.

We finally turn to a brief assessment of the nonlocal hole−vibration coupling (a detailed description of the methodology can be found in our recent work[37]). In the case of DTT-2I, we specifically investigated whether nonlocal interactions might enhance the electronic coupling between molecular π-stacks, since this would lead to a three-dimensional charge-transport character. We found that, even at room temperature, these interactions result in a rather modest variation in interstack transfer integrals, by about ±10 meV (see the Supporting Information). Thus, nonlocal vibrational coupling appears to be too weak to result in any significant vibration-assisted contribution to hole transport across molecular π-stacks (although this term is expected to affect the temperature dependence of the mobility along the π-stacks).

III. Conclusions

We have investigated the optical and electronic properties of the newly synthesized 2,6-diiododithieno[3,2-*b*:2′,3′-*d*]thiophene

and of its parent compound dithieno[3,2-*b*:2′,3′-*d*]thiophene. DFT calculations of the frontier molecular orbitals and excited states indicate that the red shift of the optical band maximum observed upon iodine substitution is due to a lowering of the LUMO energy, resulting from the inductive effect of the iodine atoms, while the HOMO remains at more or less the same energy due to the cancellation of inductive and mesomeric effects. Electrochemical data suggest that the condensed-phase ionization potentials of DTT and DTT-2I are similar and that reduction of DTT-2I leads to a cleavage of the C−I bonds.

DTT-2I presents a crystal structure reminiscent of that of α,α′-bis(dithieno[3,2-*b*:2′,3′-*d*]thiophene) with both systems displaying π-stacks along the *b*-axis. The band-structure calculations emphasize that hole transport in the DTT-2I crystal is favorable only along the π-stacking direction. This is in contrast with the 1,4-diiodobenzene crystal where the electronic couplings are determined by strong iodine−iodine intermolecular interactions.

While the calculated effective mass for holes in DTT-2I is comparable to that in the pentacene crystal, the reorganization energy in DTT-2I is 3 times larger than in pentacene; these results point to a room-temperature hole mobility in DTT-2I likely smaller than that in pentacene (as is also the case for bis-DTT). However, if we make the comparison to the parent DTT compound, iodine substitution in DTT-2I leads to a marked decrease in reorganization energy and in the formation of π-stacks, which underlines that the charge-transport parameters in DTT-2I are more favorable than those in DTT. Taken together with the data on 1,4-diiodobenzene, the results of the present work suggest that halogenation remains an interesting route for the development of new organic systems with enhanced charge transport properties.

IV. Experimental Section

A. Computational Methodology. The geometric and electronic structures of the isolated DTT and DTT-2I molecules were obtained at the density functional theory (DFT) level by performing geometry optimizations with the B3LYP functional and the 6-31G(d,p) basis set for the carbon, sulfur, and hydrogen atoms and the 3-21G(d,p) basis set for the iodine atoms, as implemented in the Gaussian package.[46] The time-dependent density functional theory (TDDFT) calculations were carried out at the same level of theory. Additional calculations, using the 6-311++G(d,p) diffuse functions for C and H atoms and the 6-311G basis set augmented by two polarization (d and f) and two (s and p) diffuse functions for the iodine atoms,[47] were carried out in the case of the radical-anion states. The results of vibration calculations, performed at the B3LYP/6-31G(d,p) level of theory, were used to calculate the relaxation energy with the DUSHIN code.[48]

The electronic-structure calculations of the DTT and DTT-2I crystals were performed at the DFT level with the PBE[49] (Perdew−Burke−Ernzerhof) exchange-correlation functional and plane-wave basis set as implemented in the VASP code.[50−52] Electron−ion interactions were described using the projector augmented wave (PAW) method.[53,54] The kinetic energy cutoff on the wave function expansion was 300 eV. The self-consistent calculations were carried out with 6 × 6 × 12 and 6 × 14 × 4 *k*-point meshes for DTT and DTT-2I, respectively. The inverse effective mass tensor was calculated using Sperling's centered difference method at the band edges with $dk = 0.02$ (2π/Å) in both molecular crystals.

The calculation of the optical vibrations at the Γ-point for the crystal structure of DTT-2I was performed using the CRYSTAL06 package.[55] In these calculations, the B3LYP

functional with a 6-31G basis set (3-21G for the iodine atoms) and a uniform $6 \times 6 \times 6$ Monkhost−Pack k-point mesh were employed.

Finally, the transfer integrals for nearest-neighbor pairs of molecules at the optimized crystal geometry were evaluated by using a fragment-orbital approach[56] in combination with a basis set orthogonalization procedure.[57] These calculations were performed with the PW91 functional and Slater-type triple-ζ plus polarization (TZP) basis sets for all atoms, using the ADF (Amsterdam Density Functional) package.[58]

B. Synthesis. Starting materials were reagent grade and were used without further purification unless otherwise indicated. Starting materials were purchased from Acros Organics unless otherwise stated. Elemental analyses were performed by Atlantic Microlabs. Mass spec (FAB) was performed on a VG Instruments 70SE. UV−vis and −NIR spectra were recorded in 1 cm cells using a Varian Cary 5E spectrometer.

2,6-Diiododithieno[3,2-b:2′,3′-d]thiophene (see Scheme 1). Acetic acid (10 mL) and chloroform (10 mL) were added to a 100 mL round-bottomed flask, which was then wrapped with aluminum foil and immersed in an ice−water bath. Dithieno[3,2-b:2′,3′-d]thiophene (synthesized according to the literature procedure[21]) (0.20 g, 1.0 mmol) was added, followed by *N*-iodosuccinimide (0.45 g, 2.0 mmol). After an hour of stirring, the reaction flask was removed from the cold bath. After 1 h, dichloromethane (200 mL) was added, and the organic layer was washed with aqueous sodium carbonate (1 × 200 mL) and water (1 × 200 mL), and was then dried with anhydrous magnesium sulfate. After filtration, the solution was concentrated by rotary evaporation to obtain a white solid, which was recrystallized from toluene to obtain olive-colored crystals, 0.36 g (80%). ^{1}H NMR (300 MHz, C$_6$D$_6$) δ 6.64 (s, 2H). ^{1}H NMR (300 MHz, CD$_2$Cl$_2$) δ 7.46 (s, 2H). ^{13}C{^{1}H} NMR (125 MHz, C$_6$D$_6$) δ 141.0, 135.2, 129.4, 73.2. MS-EI (*m/z*): 447.7 (M$^+$). Anal. Calcd for C$_8$H$_2$I$_2$S$_2$: C, 21.44; H, 0.45. Found: C, 21.54; H, 0.41.

C. Electrochemistry. Electrochemical measurements were carried out under nitrogen on dry deoxygenated DMF solutions ca. 10^{-4}–10^{-3} M in analyte and 0.1 M in tetra-*n*-butylammonium hexafluorophosphate using a BAS 100 B/W potentiostat, a glassy carbon working electrode, a platinum auxiliary electrode, and, as a pseudoreference electrode, a silver wire anodized in 1 M aqueous potassium chloride. Potentials were referenced to ferrocenium/ferrocene by using internal ferrocene. Cyclic voltammograms were recorded at scan rates of 50−2000 mV s^{-1}.

D. Single-Crystal X-ray Crystallography. Single crystals of DTT-2I (fw = 448.08) were grown from toluene, and a 0.5 × 0.07 × 0.04 mm needle was selected. Diffraction data were collected at 100 K on a Bruker APEXII diffractometer with an area CCD detector using Mo Kα radiation (0.71073 Å).[59] Cell refinement and data reduction were carried out with the Bruker SAINT-Plus program.[60] The crystal was found to belong to the monoclinic space group $P2_1/n$ with $a = 13.223(9)$ Å, $b = 4.161(3)$ Å, $c = 19.785(14)$ Å, $\beta = 96.339(10)°$, $V = 1081.9(13)$ Å^3, $Z = 4$, $\rho_{calc} = 2.751$ g cm^{-3}, $F(000) = 816$, and $\mu = 6.34$ mm^{-1}. The semiempirical method SADABS was applied for absorption correction.[61] The structure was solved by direct methods and refined by full matrix least squares on F^2 (2872 unique reflections, 2001 with $I > 2\sigma(I)$, 118 parameters) in the anisotropic approximation for all non-hydrogen atoms and was carried out with the SHELXTL NT program package.[62] The two H atoms were included using the riding-model approximation, with C−H = 0.95 Å and with $U_{iso}(H) = 1.2U_{eq}(C)$. The

refinement converged with $wR_2 = 0.152$ (all data), $R_1(I > 2\sigma(I)) = 0.0635$, and $S = 1.052$.

Supporting Information Available: Crystallographic information file (CIF) for DTT-2I; illustration of the frontier molecular orbitals of DTT-2I; DFT estimates of the relaxation energy related to hole transport in DTT and DTT-2I; and DFT estimates of the nonlocal hole−phonon coupling constants in DTT-2I. This material is available free of charge via the Internet at http://pubs.acs.org.

References and Notes

(1) Anthony, J. E. *Chem. Rev.* **2006**, *106*, 5028–5048.

(2) Bendikov, M.; Wudl, F.; Perepichka, D. F. *Chem. Rev.* **2004**, *104*, 4891–4945.

(3) Fichou, D.; Bachet, B.; Demanze, F.; Billy, I.; Horowitz, G.; Garnier, F. *Adv. Mater.* **1996**, *8*, 500–504.

(4) Garnier, F.; Horowitz, G.; Peng, X. H.; Fichou, D. *Adv. Mater.* **1990**, *2*, 592–594.

(5) Mishra, A.; Ma, C. Q.; Bauerle, P. *Chem. Rev.* **2009**, *109*, 1141–1276.

(6) Lee, S.; Koo, B.; Shin, J.; Lee, E.; Park, H.; Kim, H. *Appl. Phys. Lett.* **2006**, *88*, 162109.

(7) Torsi, L.; Dodabalapur, A.; Rothberg, L. J.; Fung, A. W. P.; Katz, H. E. *Science* **1996**, *272*, 1462–1464.

(8) Torsi, L.; Dodabalapur, A.; Rothberg, L. J.; Fung, A. W. P.; Katz, H. E. *Phys. Rev. B* **1998**, *57*, 2271–2275.

(9) Anthony, J. E. *Angew. Chem., Int. Ed.* **2008**, *47*, 452–483.

(10) Chen, M. C.; Kim, C.; Chen, S. Y.; Chiang, Y. J.; Chung, M. C.; Facchetti, A.; Marks, T. J. *J. Mater. Chem.* **2008**, *18*, 1029–1036.

(11) Tang, M. L.; Reichardt, A. D.; Miyaki, N.; Stoltenberg, R. M.; Bao, Z. *J. Am. Chem. Soc.* **2008**, *130*, 6064–6065.

(12) Valiyev, F.; Hu, W. S.; Chen, H. Y.; Kuo, M. Y.; Chao, I.; Tao, Y. T. *Chem. Mater.* **2007**, *19*, 3018–3026.

(13) Cicoira, F.; Santato, C.; Melucci, M.; Favaretto, L.; Gazzano, M.; Muccini, M.; Barbarella, G. *Adv. Mater.* **2006**, *18*, 169–174.

(14) Hunziker, C.; Zhan, X.; Losio, P. A.; Figi, H.; Kwon, O. P.; Barlow, S.; Guenter, P.; Marder, S. R. *J. Mater. Chem.* **2007**, *17*, 4972–4979.

(15) Iosip, M. D.; Destri, S.; Pasini, M.; Porzio, W.; Pernstich, K. P.; Batlogg, B. *Synth. Met.* **2004**, *146*, 251–257.

(16) Li, X. C.; Sirringhaus, H.; Garnier, F.; Holmes, A. B.; Moratti, S. C.; Feeder, N.; Clegg, W.; Teat, S. J.; Friend, R. H. *J. Am. Chem. Soc.* **1998**, *120*, 2206–2207.

(17) Odom, S. A.; Lancaster, K.; Beverina, L.; Lefler, K. M.; Thompson, N. J.; Coropceanu, V.; Brédas, J. L.; Marder, S. R.; Barlow, S. *Chem.—Eur. J.* **2007**, *13*, 9637–9646.

(18) Zhan, X. W.; Tan, Z. A.; Domercq, B.; An, Z. S.; Zhang, X.; Barlow, S.; Li, Y. F.; Zhu, D. B.; Kippelen, B.; Marder, S. R. *J. Am. Chem. Soc.* **2007**, *129*, 7246–7247.

(19) Ellman, B.; Nene, S.; Semyonov, A. N.; Twieg, R. J. *Adv. Mater.* **2006**, *18*, 2284–2288.

(20) Sánchez-Carrera, R. S.; Coropceanu, V.; Kim, E. G.; Brédas, J. L. *Chem. Mater.* **2008**, *20*, 5832–5838.

(21) Frey, J.; Bond, A. D.; Holmes, A. B. *Chem. Commun.* **2002**, 2424–2425.

(22) Roncali, J. *J. Mater. Chem.* **1999**, *9*, 1875–1893.

(23) Andrieux, C. P.; Blocman, C.; Dumasbouchiat, J. M.; Saveant, J. M. *J. Am. Chem. Soc.* **1979**, *101*, 3431–3441.

(24) Bartak, D. E.; Rudy, B. C.; Hawley, M. D.; Houser, K. J. *J. Am. Chem. Soc.* **1972**, *94*, 7526–7530.

(25) Sanecki, P. *Comput. Chem.* **2001**, *25*, 521–539.

(26) The original data were reported vs SCE and were converted using a value of +0.45 V vs. SCE for $E_{1/2}$(FeCp$_2$$^+$/FeCp$_2$) in DMF. Connelly, N. G.; Geiger, W. E. *Chem. Rev.* **1996**, *96*, 877–910.

(27) Brédas, J. L.; Silbey, R.; Boudreaux, D. S.; Chance, R. R. *J. Am. Chem. Soc.* **1983**, *105*, 6555–6559.

(28) Koepp, H. M.; Wendt, H.; Strehlow, H. *Z. Elektrochem.* **1960**, *64*, 483–491.

(29) Sato, N.; Mazaki, Y.; Kobayashi, K.; Kobayashi, T. *J. Chem. Soc., Perkin Trans. 2* **1992**, 765–770.

(30) Silins, E.; Cápek, V. *Organic molecular crystals: interaction, localization, and transport phenomena*; American Institute of Physics: New York, 1994.

Electronic Properties of DTT-2I

J. Phys. Chem. B, Vol. 114, No. 2, 2010 **755**

(31) Bertinelli, F.; Palmieri, P.; Stremmenos, C.; Pelizzi, G.; Tallani, C. *J. Phys. Chem.* **1983**, *87*, 2317–2322.

(32) Cornil, J.; Calbert, J. P.; Beljonne, D.; Silbey, R.; Bredas, J. L. *Adv. Mater.* **2000**, *12*, 978–983.

(33) Kitamura, M.; Arakawa, Y. *J. Phys.: Condens. Matter* **2008**, *20*, 184011.

(34) Brédas, J. L.; Beljonne, D.; Coropceanu, V.; Cornil, J. *Chem. Rev.* **2004**, *104*, 4971–5003.

(35) Coropceanu, V.; Cornil, J.; da Silva Filho, D. A.; Olivier, Y.; Silbey, R.; Brédas, J. L. *Chem. Rev.* **2007**, *107*, 926–952.

(36) Pope, M.; Swenberg, C. E.; Pope, M. *Electronic processes in organic crystals and polymers*, 2nd ed.; Oxford University Press: New York, 1999.

(37) Coropceanu, V.; Sánchez-Carrera, R. S.; Paramonov, P.; Day, G. M.; Brédas, J. L. *J. Phys. Chem. C* **2009**, *113*, 4679–4686.

(38) Hannewald, K.; Stojanovic, V. M.; Schellekens, J. M. T.; Bobbert, P. A.; Kresse, G.; Hafner, J. *Phys. Rev. B* **2004**, *69*, 075211.

(39) Kwiatkowski, J. J.; Frost, J. M.; Kirkpatrick, J.; Nelson, J. *J. Phys. Chem. A* **2008**, *112*, 9113–9117.

(40) Wang, L. J.; Peng, Q.; Li, Q. K.; Shuai, Z. *J. Chem. Phys.* **2007**, *127*, 044506.

(41) Norton, J. E.; Brédas, J. L. *J. Am. Chem. Soc.* **2008**, *130*, 12377–12384.

(42) Malagoli, M.; Coropceanu, V.; da Silva Filho, D. A.; Brédas, J. L. *J. Chem. Phys.* **2004**, *120*, 7490–7496.

(43) Coropceanu, V.; Kwon, O.; Wex, B.; Kaafarani, B. R.; Gruhn, N. E.; Durivage, J. C.; Neckers, D. C.; Brédas, J. L. *Chem.—Eur. J.* **2006**, *12*, 2073–2080.

(44) Bersuker, I. B. *The Jahn-Teller effect*; Cambridge University Press: Cambridge, UK; New York, 2006.

(45) Kato, T.; Yamabe, T. *J. Chem. Phys.* **2005**, *123*, 024301.

(46) Frisch, M. J.; Trucks, G. W.; Schlegel, H. B.; Scuseria, G. E.; Robb, M. A.; Cheeseman, J. R.; Montgomery, J. A., Jr.; Vreven, T.; Kudin, K. N.; Burant, J. C.; Millam, J. M.; Iyengar, S. S.; Tomasi, J.; Barone, V.; Mennucci, B.; Cossi, M.; Scalmani, G.; Rega, N.; Petersson, G. A.; Nakatsuji, H.; Hada, M.; Ehara, M.; Toyota, K.; Fukuda, R.; Hasegawa, J.; Ishida, M.; Nakajima, T.; Honda, Y.; Kitao, O.; Nakai, H.; Klene, M.; Li, X.; Knox, J. E.; Hratchian, H. P.; Cross, J. B.; Bakken, V.; Adamo, C.; Jaramillo, J.; Gomperts, R.; Stratmann, R. E.; Yazyev, O.; Austin, A. J.; Cammi, R.; Pomelli, C.; Ochterski, J. W.; Ayala, P. Y.; Morokuma, K.; Voth, G. A.; Salvador, P.; Dannenberg, J. J.; Zakrzewski, V. G.; Dapprich, S.; Daniels, A. D.; Strain, M. C.; Farkas, O.; Malick, D. K.; Rabuck, A. D.; Raghavachari, K.; Foresman, J. B.; Ortiz, J. V.; Cui, Q.; Baboul, A. G.; Clifford, S.; Cioslowski, J.; Stefanov, B. B.; Liu, G.; Liashenko, A. Piskorz, P.; Komaromi, I.; Martin R. L.; Fox, D. J.; Keith, T.; Al-Laham, M. A.; Peng, C. Y.; Nanayakkara, A.; Challacombe, M.; Gill, P. M. W.; Johnson, B.; Chen, W.; Wong, M. W.; Gonzalez, C.; Pople, J. A. Gaussian 03, revision C.02; Gaussian, Inc.: Wallingford, CT, 2004.

(47) Glukhovtsev, M. N.; Pross, A.; Mcgrath, M. P.; Radom, L. *J. Chem. Phys.* **1995**, *103*, 1878–1885.

(48) Reimers, J. R. *J. Chem. Phys.* **2001**, *115*, 9103–9109.

(49) Perdew, J. P.; Burke, K.; Ernzerhof, M. *Phys. Rev. Lett.* **1996**, *77*, 3865–3868.

(50) Kresse, G.; Furthmuller, J. *Comput. Mater. Sci.* **1996**, *6*, 15–50.

(51) Kresse, G.; Hafner, J. *Phys. Rev. B* **1993**, *47*, 558.

(52) Kresse, G.; Hafner, J. *Phys. Rev. B* **1994**, *49*, 14251.

(53) Blochl, P. E. *Phys. Rev. B* **1994**, *50*, 17953–17979.

(54) Kresse, G.; Joubert, D. *Phys. Rev. B* **1999**, *59*, 1758–1775.

(55) Dovesi, R.; Saunders, V. R.; Roetti, C.; Orlando, R.; Zicovich-Wilson, C. M.; Pascale, F.; Civalleri, B.; Doll, K.; Harrison, N. M.; Bush, I. J.; D'arco, P.; Llunell, M. *CRYSTAL06*; University of Torino: Torino, Italy, 2006.

(56) Senthilkumar, K.; Grozema, F. C.; Bickelhaupt, F. M.; Siebbeles, L. D. A. *J. Chem. Phys.* **2003**, *119*, 9809–9817.

(57) Valeev, E. F.; Coropceanu, V.; da Silva Filho, D. A.; Salman, S.; Brédas, J. L. *J. Am. Chem. Soc.* **2006**, *128*, 9882–9886.

(58) *ADF, 2005.01*; Scientific Computing and Modeling NV: Amsterdam, The Netherlands, 2005.

(59) *APEXII, Version 1.27*; Bruker AXS Inc.: Madison, WI, 2005.

(60) *SAINT-Plus for NT, Version 6.2*; Bruker AXS Inc.: Madison, WI, 2001.

(61) Sheldrick, G. M. *SADABS, Version 2.03*; Bruker AXS Inc.: Madison, WI, 2003.

(62) Sheldrick, G. M. *SHELXTL for NT, Version 6.12*; Bruker AXS Inc.: Madison, WI, 2001.